Inter Azimuth Coherence Attribute for Fracture Detection

Saleh Al-Dossary, Yves Simon and Kurt Marfurt, Allied Geophysical Laboratories, University of Houston*

Summary

Fractures occur on many scales in the earth. Fractures on a sub-seismic scale of less than tens of meters are of great interest in a reservoir context. Locating areas of greatest fracture density and determining the orientation of these fractures within a reservoir represents a significant technical challenge for geophysicists. 3-D surface seismic data can image fractures and faults more effectively if they are sorted into common azimuth bins and analyzed separately for each azimuth bin. Based on this fact, we have developed a new algorithm to detect sub-seismic faults and fractures by calculating coherence cubes *between* prestack limited azimuth seismic data. The new algorithm will calculate coherence in prestack azimuth-sorted space, rather than poststack full azimuth space. We have applied our algorithm to a survey over a fractured reservoir in Texas, with interesting results.

Introduction

Natural fractures play an important role in petroleum exploration. Fractures are found in almost every reservoir, rock type, and depth. Petroleum explorationists pay a great deal of attention to locating these fractures in order to understand the reservoirs. Fractures can advance or hinder the effort in understanding reservoir character. Fractures can be found in source rocks, reservoir rocks and cap rocks. Locating these fractures and identifying their orientation can help the explorationists to deal with them and benefit from their presence or avoid their annoyances.

The use of seismic coherence to detect fractures has been investigated since the first emergence of the coherence cube as a new attribute of seismic data. Estimates of seismic coherence (e.g. Bahorich and Farmer, 1995; Marfurt et al, 1998, Gertzenkorn and Marfurt, 1999; Marfurt and Kirlin, 2000) provide a quantitative measure of the changes in waveform across a discontinuity. Estimates of apparent dip (e.g. Dalley et al, 1989; Luo et al., 1996; Marfurt et al, 1998; Marfurt and Kirlin, 2000; Luo et al, 2001) provide a measure of change in reflector dip/azimuth across a discontinuity. Estimates of amplitude gradients (e.g. Luo et al., 1996; Marfurt and Kirlin, 2000) provide a measure of changes in reflectivity across a discontinuity. More recently Al-Dossary and Marfurt (2004) have used spectrally limited volumetric curvature to help predict fractures. Skirius et al. (1999) used seismic coherence in carbonates in North America and the Arabian Gulf to detect fault and fractures. Luo et al. (2002) showed some examples from a Saudi Arabian carbonate field where amplitude gradients have helped in delineating fractures. These investigations, however, have all been made using post stack data. In their work, Chopra et al. (2000) applied a fairly simple process of sorting the data according to source-receiver azimuth bins by migrating the partially stacked data, and applying coherence to each volume. In general, stacking all the data into a single volume using an inaccurate velocity smears the data, thereby increasing the overall coherence of the image, blurring edges and other discontinuities. While having lower fold and hence exhibiting lower signal to noise ratios, Chopra et al's (2000) common azimuth images show better definition of edges inferred to be microfaulting or fractures. We have developed a new algorithm to detect fractures by calculating coherence between prestack data volumes. We will calculate coherence on the traces of the same offset but of different azimuth. The offsets we will work with are the near (0° to 20°) and the far (>20°), and the azimuths (NE and NW) are approximately parallel and perpendicular to expected fractures.

Algorithm Description

Azimuthal variations caused by fracture-induced anisotropy affect P-wave attributes such as traveltime, amplitude and velocity (Lynn et al, 1996)

To implement our algorithm, we have sorted the data according to azimuth (parallel and perpendicular) and to offsets (near and far), generating four subvolumes:

1. Parallel azimuth and near offset (subvolume1),
2. Perpendicular azimuth and near offset (subvolume2),
3. Parallel azimuth and far offset (subvolume3), and
4. Perpendicular azimuth and far offset (subvolume4).

We then calculated coherence between traces having the same offset, but with different azimuth.

Model

To illustrate our methodology, we have generated a simple 2-D model. The model consists of three horizontal layers. The first and the third layers are isotropic. The middle layer (fractured layer) includes azimuthally anisotropic zones (Figure 1a). Figures 1b, 1d and 1e depict the seismic responses. The 25 meter thick layer is below resolution, and only one series of peaks is visible. Figure 1c and 1f depict the result of cross correlating the traces from the parallel azimuth dataset against those from the perpendicular azimuth dataset. The results for fractures inside a 25 meter thick layer, where detecting changes by interval velocity analysis becomes intractable, are very similar to those for a 100 meter thick layer.

Field Data

We now apply our algorithm to seismic data from a 3D-wide azimuth survey over a fractured reservoir in Texas. In Figure 2, we display time slices through two of the four volumes. Figure 3 shows the waveform changes between NE and NW volumes, for the near and the far data sets.
Unlike other attributes, the cross-correlation between NE and NW volumes shows lineation oriented NW-SE and NE-SW in the reservoir. This is very encouraging, as the natural stress is oriented NE-SW, and micro-fractures detected in cores are oriented NW-SE (the stress direction has changed with time).
We found only a small, but significant, linear inverse correlation by cross plots with production data of 110 wells. We are investigating possible geologic explanations of these results, and will test our new algorithm with more sophisticated, spatial statistical tools (e.g., co-kriging) against other seismic attributes and physical measurements.

Conclusions

We have developed a new algorithm for direct detection of azimuthal anisotropy that can provide insight necessary to characterize fracture systems, stress anisotropy, and potential permeability directions.
We have applied this new algorithm on modeled and field data sorted in two azimuths at ninety degrees to each other and same limited offsets (near or far), with interesting results.
In addition to avoiding manual velocity picking we believe that our methodology can provide sensitive tool to identify fractures within layer thickness smaller than seismic wavelength.

References

Al-Dossary, S., and Marfurt, K. J., 2004, 3-D volumetric multispectral estimates of reflector curvature and rotation, submitted to Geophysics.

Bahorich, M.S., and Farmer, S.L., 1995, 3-D seismic discontinuity for faults and stratigraphic features: The coherence cube, The leading Edge, 1053-1058.

Chopra, S., Sudhakar, V., Larsen, G., and Leong, H., 2002, Azimuth-based coherence for detecting faults and fractures: World Oil Magazine, 21.

Dalley, R M., Gevers, E. E. A., Stampli, G. M., Davies, D. J., Gastaldi, C. N., Ruijetnberg, P. R., and Vermeer, G. J. D., 1989, Dip and azimuth displays for 3-D seismic interpretation: First Break, 7, 86-95.

Gersztenkorn, A., and Marfurt, K. J., 1999, Eigenstructure based coherence computations: Geophysics, 64, 1468–1479.

Luo, Y., Higgs, W. G. and Kowalik, W. S., 1996, Edge detection and stratigraphic analysis using 3-D seismic data, 66th Ann. Inter. Mtg. Soc. Expl. Geophys. Expanded Abstract, 324-327.

Luo, Y., Al-Dossary, S. and Marhoon, M., 2001 Generalized Hilbert transform and its application in Geophysics, 71th Ann. Mtg. Soc. Expl. Geophys. Expanded Abstract, 430-434

Luo, Y., Marhoon M., Al-Dossary S., and Alfaraj, M., 2001 Edge-Preserving Smoothing and its application in Geophysics, 71th Ann. Mtg. Soc. Expl. Geophys. Expanded Abstract, 370-374

Lynn, H. B., Simon, K. M., and Bates, C. R., 1996, Correlation between P-wave AVOA and S-wave traveltime anisotropy in a naturally fractured gas reservoir: The Leading Edge, **15**, 931–935.

Marfurt, K. J., and Duncan, W., 2002 Comparison of 3-d edge detection seismic attributes to Vinton Dome Louisiana: 72nd Ann. Internat. Mtg., Soc. Expl. Geophys.,Expanded Abstracts, 723–730.

Marfurt, K. J., Kirlin, R. L, Farmer, S.L., and Bahorich, M.S., 1998, 3-D seismic attributes using a semblance-based coherency algorithm: Geophysics, **63**, 1150-1165.

Marfurt, K, J, and Kirlin, R. L., 2000, 3-D broad-band estimates of reflector dip and amplitude: Geophysics, **65**, 304-320

Skrius, C., Nissen, S., Haskell, N., Marfurt, K. J., Hadley, S., Ternes, D., Michel, K., Reglar, I., D'Amico, D., Deliencourt, F., Romero, T,. Romero, R., and Brown, B., 1999, 3-D seismic attributes applied to carbonates: The Leading Edge, **18**, 384-389

Acknowledgments

The authors thank the sponsors of AGL as well as Devon Energy and Lynn Inc. for data and support.
The first author wishes to thank Saudi Aramco for the opportunity and support in pursuing his graduate studies, and especially Dr. Yi luo.

Inter Azimuth Coherence Attribute for Fracture Detection

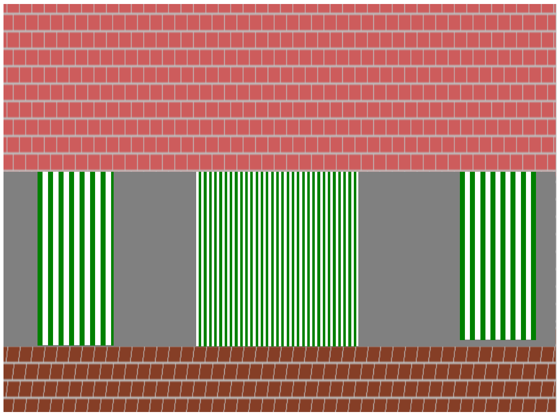

Fig. 1a: Model with aligned fractures, thickness of central layer 25 or 100 meters

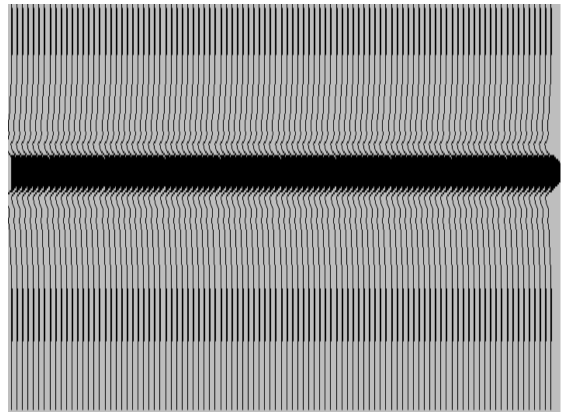

Fig. 1d: Seismic response, source-receiver parallel to fractures, 25 meters thickness

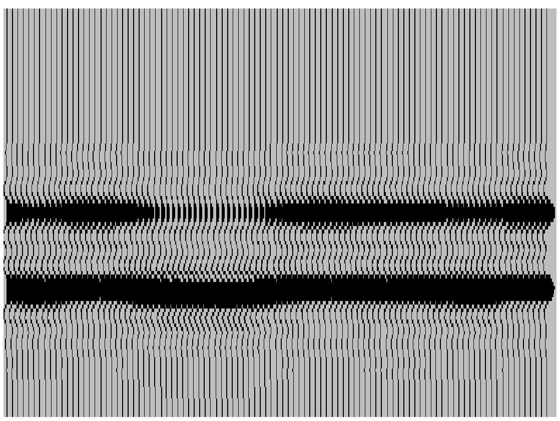

Fig. 1b: Seismic response, source-receiver perpendicular to fractures, 100 meters thickness

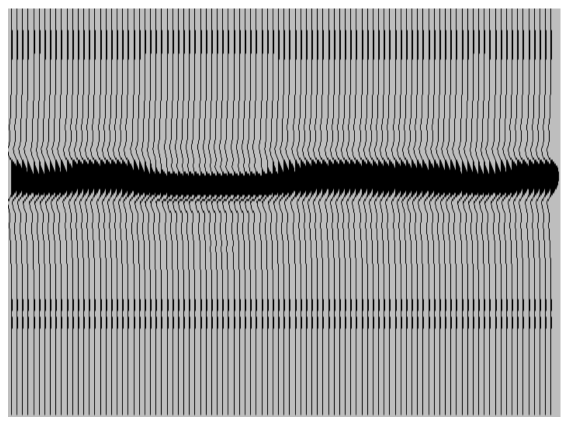

Fig. 1e: Seismic response, source-receiver perpendicular to fractures, 25 meters thickness

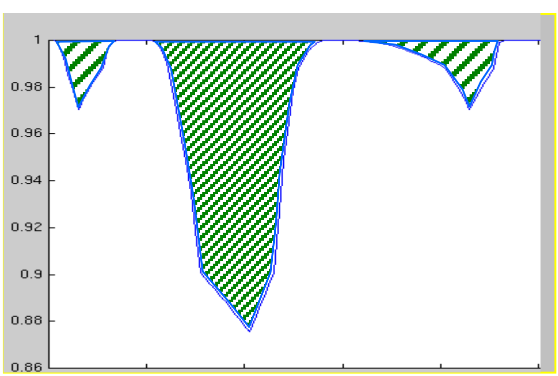

Fig. 1c: Cross-correlation of the traces from parallel azimuth dataset against those from perpendicular azimuth dataset ; 100 meters thickness

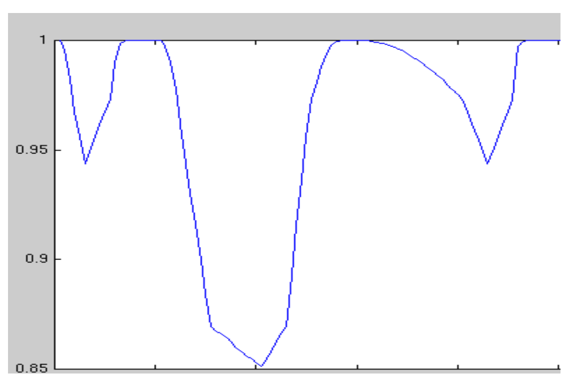

Fig. 1f: Cross-correlation of the traces from parallel azimuth dataset against those from perpendicular azimuth dataset ; 25 meters thickness

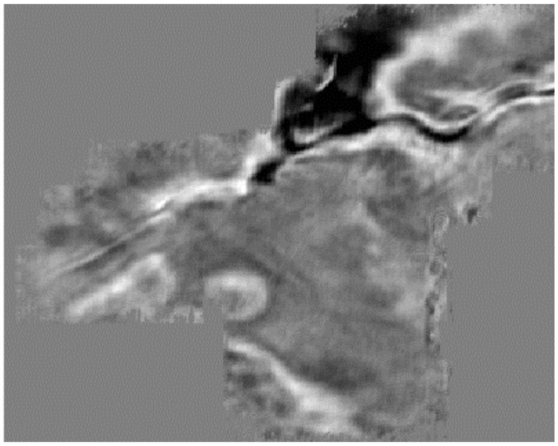

Fig. 2a: Time slice of NW near

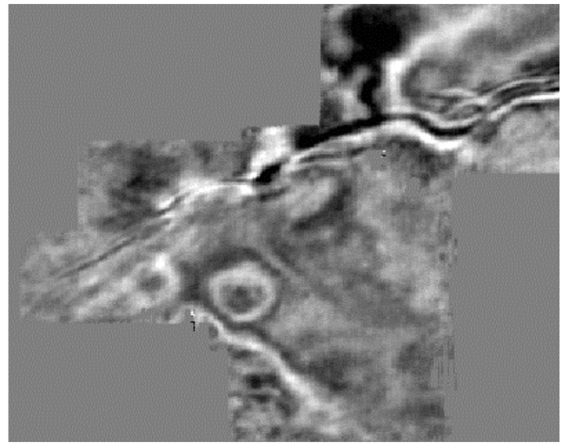

Fig. 2b : Time slice of NE far

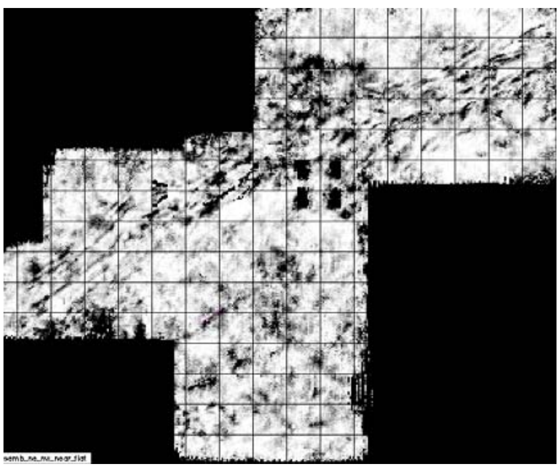

Fig. 3a: Coherence between NE and NW dataset, near offsets

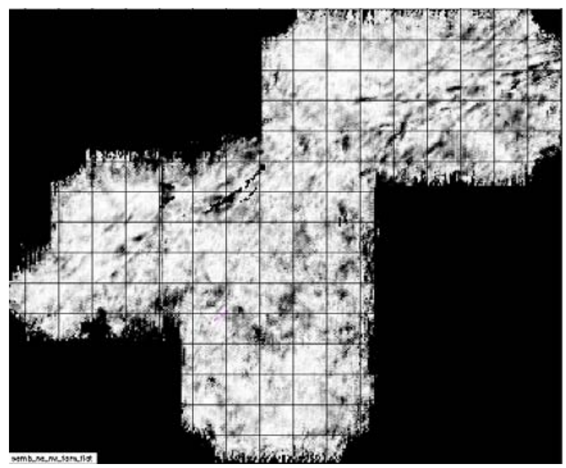

Fig. 3b: Coherence between NE and NW dataset, far offsets

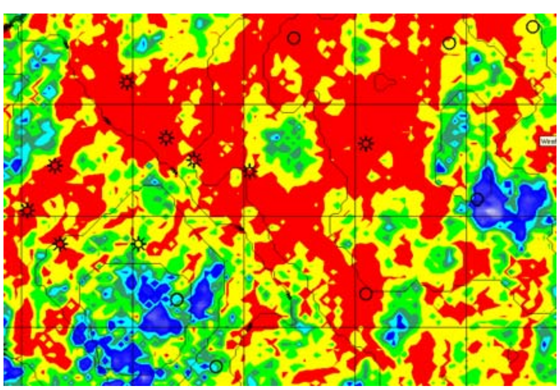

Fig.4: Coherence between NE and NW dataset, near offset, 7 samples (24 ms) ; Warm colors, coherent traces ; Cold colors, incoherent traces ; Best and worst producing wells displayed